Published in final edited form as:
J Cereb Blood Flow Metab. 2009 April ; 29(4): 738–751. doi:10.1038/jcbfm.2008.166.

Active dilation of penetrating arterioles restores red blood cell flux to penumbral neocortex after focal stroke

Andy Y. Shih, Ph.D.[1], **Beth Friedman, Ph.D.**[2], **Patrick J. Drew, Ph.D.**[1], **Philbert S. Tsai, Ph.D.**[1], **Patrick D. Lyden, M.D.**[2,3], and **David Kleinfeld, Ph.D.**[1,3]

[1]Department of Physics, University of California at San Diego, La Jolla, CA 92093

[2]Department of Neuroscience, University of California at San Diego, La Jolla, CA 92093

[3]Graduate Program in Neurosciences, University of California at San Diego, La Jolla, CA 92093

Abstract

Pial arterioles actively change diameter to regulate blood flow to the cortex. However, it is unclear whether arteriole reactivity and its homeostatic role of conserving red blood cell (RBC) flux remains intact after a transient period of ischemia. To examine this issue, we measured vasodynamics in pial arteriole networks that overlie the stroke penumbra during transient middle cerebral artery occlusion in rat. *In vivo* two-photon laser-scanning microscopy was used to obtain direct and repeated measurements of RBC velocity and lumen diameter of individual arterioles, from which the flux of RBCs was calculated. We observed that occlusion altered surface arteriole flow patterns in a manner that ensured undisrupted flow to penetrating arterioles throughout the imaging field. Small diameter arterioles (< 23 μm), which included 88% of all penetrating arterioles, exhibited robust vasodilation over a 90 min occlusion period. Critically, persistent vasodilation compensated for an incomplete recovery of RBC velocity during reperfusion to enable a complete restoration of post-ischemic RBC flux. Further, histological examination of tissue hypoxia suggested re-oxygenation through all cortical layers of the penumbra. These findings indicate that selective reactivity of small pial arterioles is preserved in the stroke penumbra and act to conserve RBC flux during reperfusion.

Keywords

Homeostasis; ischemia; rodent; two-photon microscopy; vasculature

The *in vivo* examination of blood flow in single arterioles has been a valuable approach to studying vascular function under normal and pathological conditions. In rat, the perfusion of each cubic millimeter of neocortex is strictly regulated by ten or more penetrating arterioles (Nishimura et al. 2007), which are in turn supplied by a highly interconnected plexus of surface arterioles with heterogeneous flow profiles (Bar 1980; Schaffer et al. 2006). The vascular response to change in neuronal input (Devor et al. 2007) or to disruption of blood flow (Kontos et al. 1978), involves populations of arterioles that react differently based on their size and location within the network. Thus, examination of blood flow on the level of individual vessels is necessary to characterize these responses.

Red blood cell (RBC) velocity in pial arterioles is, on average, an order of magnitude faster than in capillaries. Using confocal or two-photon laser scanning microscopy (TPLSM), RBC

Correspondence: David Kleinfeld, Department of Physics, University of California at San Diego, 9500 Gilman Drive, La Jolla, CA 92093-0374, Office: 858-822-0342, Fax: 858-534-7697, dk@physics.ucsd.edu.

Disclosures: None.

velocity can be tracked in individual arterioles using high-speed line-scans (Dirnagl et al. 1992; Kleinfeld et al. 1998), and vessel diameters determined from planar image stacks. These parameters can then be combined to determine absolute RBC flux, which provides a complete description of blood flow in each vessel (Ngai and Winn 1996; Rovainen et al. 1993; Schaffer et al. 2006).

We apply this technique to examine the important issue of whether homeostatic regulation of RBC flux is preserved in the acutely recovering stroke penumbra (Iadecola 1998). The preservation of cerebrovascular reactivity is critical for buffering variations in post-ischemic blood flow (Paulson et al. 1990), and loss of this function in humans has been linked to recurrence of stroke and poor recovery (Marshall 2004). Severe ischemia in the focal stroke core can compromise the myogenic response to changes in arteriole pressure (Cipolla et al. 2001). However, less is known about the state of arterioles in the stroke penumbra, where residual blood flow may be sufficient to preserve vascular function and improve tissue recovery following reperfusion (Dirnagl and Pulsinelli 1990; Iadecola 1998). This includes the effect of stroke on penetrating arteriole reactivity, which constitutes ~ 40% of the cerebrovascular resistance for blood flow (Cipolla et al. 2004; Heistad and Kontos 1983).

We measured the vasodynamics of flow in pial arterioles across the stroke penumbra in parietal cortex during 90 min of transient middle cerebral artery occlusion (tMCAo). We ask: *i.*) How does the pattern of RBC flow in the pial arteriole network change in response to MCA occlusion, and what is the role of these flow changes? *ii.*) Does measurement of RBC velocity or lumen diameter alone accurately predict RBC flux during stroke? *iii.*) Is compensatory arteriole reactivity intact after stroke, and are penetrating arterioles, as a population, able to maintain normal levels of flux? Importantly, these questions are not accessible to laser Doppler flowmetry (LDF), which records from multiple vessels and, in practice, is insensitive to the relatively high flow rates in pial vessels (Barfod et al. 1997). Rather, we make use of *in vivo* TPLSM to obtain systematic and repeated measurements of RBC velocity and lumen diameter in individual surface and penetrating arterioles.

Materials and Methods

Animal models and surgery

In total, 57 male Sprague Dawley rats from Charles River were used in this study, ranging in mass from 270 to 310 g. Thirteen animals were imaged during tMCAo using the ‘Koizumi’ method, *i.e.*, ipsilateral common carotid artery (CCA) ligated during reperfusion (Koizumi et al. 1986), 4 for tMCAO using the ‘Longa’ method, *i.e.*, ipsilateral CCA intact during reperfusion (Longa et al. 1989), 7 for Sham tMCAo controls, *i.e.*, ipsilateral CCA ligation and partial filament insertion (Supplemental Fig. 2), 6 for Window only controls, *i.e.*, cranial window but no vascular manipulation (Supplemental Fig. 3), 4 for hypercapnic treatment to control for large surface arteriole dilation, 12 for pimonidazole studies using the ‘Koizumi’ method, and 11 for LDF studies. Anesthesia was maintained with 1 to 2 % (v/v) isoflurane (Baxter Healthcare) in 30 % oxygen and 70 % nitrous oxide. As isoflurane is a vasodilator that can affect cerebral autoregulation (Eger 1981), the Window only group provided a control for the effects of anesthesia over time (Supplemental Fig. 3). Atropine (American Regent), 0.05 mg per kg body weight intraperitoneal, and lidocaine (Hospira Inc.), 2 % (v/v) subcutaneous, were administered at the start of surgery. Body temperature was maintained at 37°C with a feedback-regulated heat pad (50-7053-F; Harvard). Heart rate and blood oxygen saturation were continuously monitored using a pulse oximeter (8600V; Nonin). Cranial windows, 4 × 4 mm in size and centered at 4.5 mm medial-lateral and −3.0 mm anterior-posterior, were constructed as described previously (Kleinfeld et al. 2008). The left femoral artery was catheterized with polyethylene 50 tubing (Intramedic) connected to a stopcock and 10 mL syringe filled with heparin-saline (20 units per mL, Baxter Healthcare). Arterial blood was

sampled from the catheter for blood gas measurement (RapidLab 248; Bayer) during each of three imaging periods, *i.e.*, baseline, occlusion, and reperfusion. Blood pressure was measured with the tail cuff method (XBP-1000; Kent Scientific) once during each imaging period. Intraperitoneal injections of 5 % (w/v) glucose in 1 mL saline were given every 2 h for re-hydration.

Transient middle cerebral artery occlusion was induced using the intraluminal filament method. Ischemia was maintained for 90 min and followed by 90 min of reperfusion. We examined two variations of the model and exploited their differences in post-ischemic blood flow. In the majority of the experiments, the CCA was permanently ligated to generate an incomplete reperfusion (Koizumi et al. 1986). In a control study, we left the CCA intact, which generated a transient hyperemia during the reperfusion period (Longa et al. 1989). In all cases, the filament placement was guided with LDF measurements through the cranial window. Animals that exhibited sub-arachnoid hemorrhage were excluded from the study.

The penumbra was defined by the amount of residual blood flow during occlusion, typically ranging within 25-50% of baseline flow values, measured either using LDF or averaging arteriole flux measurements from the cranial window. This level of blood flow in the penumbra is a generally accepted range (Lipton 1999) and is contrasted to flow in the ischemic core, which can be lower than 20% of baseline.

Two-photon microscopy

Images were collected using a two-photon laser scanning microscope of local design (Tsai et al. 2003; Tsai et al. 2002) that was controlled by MPScope software (Nguyen et al. 2006). The blood serum was labeled using 0.3 mL of 2 MDa fluorescein-dextran (FD2000S; Sigma) prepared at a concentration of 5% (w/v) in saline, and delivered through the femoral artery catheter, with 0.1 mL supplements as required (Schaffer et al. 2006). A 0.3-numerical aperture (NA), 10-times magnification water-dipping objective (Zeiss) was used to collect a large-scale map to aid navigation through the cortical vasculature, while a 0.8-NA, 40-times magnification water-dipping objective (Olympus) was used to obtain high-resolution line-scan and planar data. The line-scans were collected along the centerline of each vessel over a length of 70 pixels, spanning 7 to 76 μm, at a scan rate of 1.6 kHz/line. RBC velocity was determined from the slope of the line-scan streaks using a method based on singular value decomposition (Kleinfeld et al. 1998). For each vessel, we reported the average velocity over a 1.5 s period. Planar image stacks, 256 by 256 pixels, were acquired to establish the diameter of the vessel. Our analysis was limited to arterioles smaller than 60 μm in diameter as a result of technical constraints. A further limitation was that penetrating arterioles could only be measured if a portion of the vessel was parallel to the cortical surface before diving perpendicularly. In a survey of 154 penetrating arterioles across 11 rats, 17% were not measurable as a result of this limitation.

During analysis of surface arterioles, a 23 μm break-point was used to divide the vessels into small and large diameter categories. This number corresponded to the intersection between normalized histograms for penetrating arteriole (n = 215) and surface arteriole (n = 271) diameters at baseline, and by maximum likelihood, was the natural point to divide the data. Further, 23 μm was the median diameter for measured surface arterioles.

Flux quantification

Under the assumption that the flow in the vessels is laminar, RBC velocity and lumen diameter collected from a single vessel can be used to define the average volume flux, $\bar{F}$, by:

$$\vec{F} = \langle \vec{v} \rangle A = \frac{\pi}{8} \vec{v}(0) d^2, \tag{1}$$

where $\langle \vec{v} \rangle$ is the average RBC velocity, A is the cross-sectional area of the vessel lumen, $\vec{v}(0)$ is the RBC velocity along the central axis of the vessel, and d is the lumen diameter. Contrawise, the condition of constant flux implies that the change in diameter, Δd, that is required to offset a change in speed, *i.e.*, $\Delta\vec{v}(0)$, is given by

$$\frac{\Delta d}{d} = \sqrt{\frac{1}{1 + \left[\Delta \vec{v}\,(0) / \vec{v}\,(0) \right]}} - 1 \xrightarrow{\Delta \vec{v}(0) \to 0} -\frac{1}{2} \frac{\Delta \vec{v}\,(0)}{\vec{v}\,(0)}. \tag{2}$$

A decrease in $\vec{v}(0)$, *i.e.*, $\Delta\vec{v}(0) < 0$, yields an increase in d, *i.e.*, $\Delta d > 0$.

Vascular casting

A fluorescent agarose gel was formulated from 0.42% (w/v) 2 MDa fluorescein-dextran and 1% (w/v) low gelling temperature agarose (A4018; Sigma) in phosphate-buffered saline (PBS), mixed at 60 °C and maintained at this temperature prior to use (Tsai 2004). Cerebral blood vessels were dilated by administration of 5 % CO_2 and 95 % O_2 with 2 % isoflurane through a nose cone for 15 min to facilitate perfusion of the gel. Animals were perfused transcardially through the left ventricle with 100 mL of PBS, 100 mL of 4% paraformaldehyde, another 50 mL of PBS to wash out residual fixative. Fifty mL of the gel was then steadily injected into the ventricle using a syringe at a rate of ~ 2 mL per second. The gel was rapidly solidified *in situ* by placing the animal in an ice bath. The brain was carefully extracted to avoid damage to pial vessels. The cortex of the ischemic hemisphere was removed and flattened between two glass slides separated by a distance of 3 mm for wide-field fluorescence microscopy (Axioplan 2; Zeiss). The arteriole network, including the region imaged *in vivo*, was traced from overlapping images taken with a 0.5-NA 10-times magnification air objective (Zeiss).

Pimonidazole immunohistochemistry

Pimonidazole hydrochloride (Hypoxyprobe™; Hypoxyprobe.com) is a sensitive method for detecting even small volumes of tissue hypoxia, *i.e.*, < 10 mm Hg tissue oxygen, compared with approximately 30 mm Hg under normoxic conditions (Nishimura et al. 2006; Takasawa et al. 2008). Pimonidazole was injected through the femoral artery catheter at a concentration of 60 mg per kg body weight. For immunostaining, 50 μm frozen sections were treated for 10 min with 3 % (v/v) H_2O_2, and incubated for 72 h in anti-Hypoxyprobe™ antibody diluted 10^3-times in PBS containing 10 % (v/v) normal goat serum (Vector Laboratories), 2 % (v/v) triton X-100 (Sigma), and 0.2 % (v/v) sodium azide (Sigma). Bound antibody was visualized with the Vectastain ABC kit and diaminobenzadine peroxidase substrate kit (both from Vector Laboratories) and brain sections were photographed using a MacroView microscope (MVX10; Zeiss). Pimonidazole staining was quantified from brain sections, originating from Bregma -3.0 mm anterior-posterior, by first determining the normalized intensity histogram for staining in both ischemic (ipsilateral) and non-ischemic (contralateral) cortices. A threshold, set to include the largest 90 % of pixel values from the non-ischemic side, was then used to isolate stained regions on the ischemic side, which was presented as a percentage of the total cortical area.

Laser Doppler flowmetry

Flowmetry measurements were performed with a MoorLab unit (Moor Instruments; λ_o = 780 nm and f_{cut} = 15 kHz low-pass filtered, to give a maximum measurable speed of $\lambda_o f_{cut} / 2$ = 6 mm/s), fitted with a MP1-V2 probe tip that was held in place with a custom adaptor over the cranial window or thinned skull. The LDF "flux" output, a measure of average RBC velocity multiplied by the intensity of the reflected signal, was collected at a sampling rate of 40 Hz using WinEDR software (http://spider.science.strath.ac.uk/sipbs/software_ses.htm), and averaged over 60 s intervals.

Statistics

Data are presented as mean ± standard error of the mean (SEM). We used the non-parametric Wilcoxon signed rank test unless otherwise stated since the *in vivo* imaging data was not always normally distributed. In Fig. 4, differences between experimental means and a theoretical line of conserved flux were tested with a two-tailed one sample t-test. In Fig. 6, differences between pimonidazole stained cortical area was analyzed with an unpaired t-test. In Fig. 7, vasodynamic changes between imaging periods were analyzed using a two-tailed paired t-test.

Results

Pial arteriole vasodynamics under basal conditions

We obtained an overview of RBC flux from surface and penetrating arterioles through a cranial window in the anesthetized rat (Figs. 1A to 1C). Line-scans were used to measure the centerline velocity (maximal velocity) of RBCs in individual arterioles, denoted $\vec{v}(0)$, followed immediately by the collection of an image stack to measure vessel diameter, d (Figs. 1D and 1E). A random sampling of surface arterioles at baseline yielded RBC velocities that ranged from 1.4 to 34 mm/s in vessels with diameters between 5 and 60 μm (Fig. 1F). The range of velocities in penetrating arterioles was similar, 0.7 to 35 mm/s, but all vessels were 30 μm or less in diameter (Fig. 1G). Velocities were significantly correlated with diameter for both surface arterioles, $r = 0.49$ ($p < 10^{-4}$), and penetrating arterioles, $r = 0.26$ ($p < 10^{-4}$). To emphasize size-based differences in our subsequent analyses, we separated the arterioles into three categories: large surface arterioles ($d > 23$ μm, *i.e.*, d greater than the median diameter of surface arterioles), small surface arterioles ($d < 23$ μm), and penetrating arterioles. The flux of RBCs (Eq. 1) in large surface arterioles ranged from 0.3 to 100 nL/s, while flux in small surface arterioles and penetrating arterioles were, on average, an order of magnitude lower, typically between 0.01 and 10 nL/s (Fig. 1H).

Pial arteriole vasodynamics in response to tMCAo

We used the intra-luminal filament model to transiently occlude the MCA origin for 90 min followed by 90 min of reperfusion (Koizumi et al. 1986). We first consider stroke-induced change in RBC flow direction within the pial network, followed by quantitative measurements of RBC velocity and lumen diameter. We then combine these parameters to assess RBC flux. Physiological parameters including blood gas, blood pressure, and core temperature were within normal limits throughout the imaging sessions (Supplemental Table 1). Unnormalized values for all measured vasodynamic parameters are provided in Supplemental Figure 1.

MCA occlusion causes RBC flow reversal in surface arterioles but not penetrating arterioles

Reversal in the flow direction or stalling in the movement of RBCs was observed in 12 % of the total measured surface arterioles during occlusion. These changes typically occurred in three network patterns: (*i*) small surface arteriole loops spanning ~ 500 μm^2 of cortical surface area (7 % of total surface arterioles) (Fig. 2A); (*ii*) direct arteriole connections between MCA and anterior cerebral artery (ACA) perfusion sources (3 %) (Fig. 2B)(Schaffer et al. 2006); and

(*iii*) "connector vessels" that balanced blood flow between major branches of the MCA (2%) (Fig. 2C). We used post-mortem analysis of fluorescent vascular casts to further evaluate the connectivity of vessels beyond the imaged region (Fig. 1A). In general, 72 % of the examined surface arterioles were located within loops or directly linked to collaterals of the ACA. Reperfusion resolved nearly all reversals and stalls in the surface network. In contrast to the case for surface arterioles, flow in the penetrating arterioles neither reversed nor stalled during the occlusion but rather responded homogeneously to the overall decrease in blood flow. As a guiding hypothesis, this suggests that flow irregularities in the surface network acts to maintain uninterrupted flow to penetrating arterioles during occlusion.

Change in RBC velocity and lumen diameter during tMCAo

The 'Koizumi' method of tMCAo involves permanent ligation of the ipsilateral CCA, which generates an incomplete recovery of blood flow during reperfusion, as detected by LDF (Fig. 3A) (Koizumi et al. 1986). We exploited this feature of the model to determine whether arteriole reactivity remains intact and capable of compensating for incomplete reperfusion.

Overall, the RBC velocity across each class of arterioles decreased to ~30 % of the baseline levels during occlusion (Fig. 3C, left panel); this degree of ischemia falls within a range defined as penumbral flow (Lipton 1999). Following 90 min of occlusion, the filament was retracted to initiate reperfusion. In eleven of thirteen experiments, reperfusion was accompanied by a substantial recovery of RBC velocities toward their baseline values (Fig. 3C, right panel). Nonetheless, the velocities across all arterioles recovered to only ~ 70 % of their baseline levels, similar to LDF measurements (Fig. 3A) (data includes 65 large surface arterioles, 56 small surface arterioles, and 75 penetrating arterioles over 11 animals).

In two cases of tMCAo, flow values were sufficiently low to be categorized as stroke core, *i.e.*, flow decrease to 17 % and 13 % of baseline levels. Recovery of RBC velocities was poor in these cases, returning to only 35 % and 38 % of baseline levels upon reperfusion, respectively, in contrast to ~70 % for the main cluster of tMCAo cases. Since these severely ischemic cases represented a small proportion of the total animals, they were removed as outliers in subsequent analyses of the data.

Lumen diameter of small surface arterioles and penetrating arterioles increased robustly by an average of ~ 20 % over baseline levels (Figs. 3B, left and center panel, and 3D, left panel) during occlusion. This vasodilation persisted into the reperfusion period (Figs. 3B, right panel, and 3D, right panel), and was observed as late as 90 min after de-occlusion, indicating a prolonged contribution to post-ischemic blood flow (data not shown). In contrast, the diameter of large surface arterioles exhibited both dilation and constriction, but on average did not change significantly from baseline at any stage during tMCAo (Fig. 3D). However, large surface arterioles dilated uniformly in response to hypercapnia, which verifies that these vessels were not already maximally dilated by generation of the cranial window (Supplemental Materials).

Vasodilation tracks RBC velocity to conserve flux after ischemia

The above results show a net increase in diameter of small surface arterioles and penetrating arterioles concomitant with the net decrease in the RBC velocity during both periods of occlusion and reperfusion. Does the change in diameter compensate for decrease in velocity to conserve RBC flux (Eq. 2)? During occlusion, the dilation was insufficient to maintain baseline levels of RBC flux through penetrating arterioles and the mean change corresponded to a significant net drop in flux ($p < 0.001$) (Fig. 4A; red box, mean ± 2 SEM, lies far from the theoretical line for conserved flux). In contrast, when reperfusion was initiated, the mean arteriole diameter remained dilated such that baseline levels of flux could be achieved despite

incomplete recovery of RBC velocity. This central result indicates that persistent vasodilation during reperfusion was an enabling factor for the complete recovery of flux to baseline levels in small arterioles (Fig. 4B; red box, mean ± 2 SEM, lies atop theoretical line for conserved flux).

To control for the effects of generating a cranial window, we also imaged a Window control group, *i.e.*, cranial window without vascular manipulation. This group showed no significant change in either diameter or velocity through two rounds of imaging, which corresponded to the same time schedule as occlusion and reperfusion in the tMCAo group, and thus no significant deviation from conserved flux was observed for the mean response (Fig. 4C and 4D) (Supplemental Figure 3). The Window control group also revealed an inherent variability in the measured parameters in individual vessels over time. Although the mean response of vessel populations collected over many animals demonstrated a clear association with the line for conserved flux, vasodynamic changes did not necessarily conform to this theory at the level of individual vessels.

To further examine the relationship between RBC flux and vessel diameter, and to verify the accuracy of our measurements, we calculated flux for all vessels in the tMCAo experiments (Eq. 1). When normalized flux was plotted as a function of lumen diameter (Fig. 5A), a clear preferential recovery of small surface arterioles and penetrating arterioles, as opposed to large surface arterioles, was observed during the reperfusion period. This is consistent with specific dilation of small diameter arterioles shown in Fig 3D.

Our claims depend on an absence of systematic errors in the determination of RBC flux. As a control, we checked if the measured input into a small network was equal to its output. Such measurements were only possible in networks where all input/output vessels had a segment parallel to the focal plane; this requirement was achieved in 2 networks (Figs. 5B and 5C). In these cases, we confirmed that flux was essentially conserved during all three imaging periods within an error range of 5 % (n = 6). As in the data with random sampling (Fig. 5A, right panel), the integrated flux through penetrating arterioles was restored to baseline levels during reperfusion while the total flux input to the network from large surface arterioles was reduced.

Reperfusion after tMCAo relieves hypoxia in penumbral cortex

To examine whether recovery of RBC flux to penetrating arterioles was consistent with tissue re-oxygenation, we examined for hypoxic tissue in the imaged region using pimonidazole accumulation as a probe of hypoxia (Takasawa et al. 2008). Consistent with previous work, pimonidazole injection during the period of occlusion led to heterogeneous staining of hypoxic cells throughout the MCA-supplied territory (Figs. 6A to 6D, left column) (Noto et al. 2006). Interestingly, blood vessels and the immediate neuropil surrounding the vessels appeared largely unlabeled in the cortex (Fig. 6C, arrowheads). In contrast to occlusion, when pimonidazole was injected immediately after the onset of reperfusion, the dorsal cortex was largely unstained, suggesting homogeneous re-oxygenation of the post-ischemic tissue (Figs. 6A to 6D, right column); we noted only sparse labeling of individual cells with neuronal morphology (Fig. 6C, right panel inset). Importantly, even after reperfusion, areas within the lateral cortex often remained labeled (Fig. 6B, right panel), which confirmed that this method was capable of detecting areas with poor reperfusion. LDF was used to ensure that a similar reduction in blood flow was achieved between occlusion-injected and reperfusion-injected groups, and that successful reperfusion was achieved in the latter group (data not shown). This result indicates that there are no poorly reperfused zones in the imaged region at surface and subsurface levels consistent with full reperfusion of penetrating arterioles.

Preserved arteriole reactivity to post-ischemic hyperemia and hypercapnia

As a final control, we tested if post-ischemic arterioles could constrict during a blood flow increase above baseline levels, *i.e.*, hyperemia. A preserved myogenic response to hyperemia would indicate an active compensatory mechanism for change in vessel diameter rather than a passive loss of smooth muscle tone. For this experiment, we used a variation of the stroke model that maintained unobstructed flow of the ipsilateral CCA during reperfusion (Longa et al. 1989). In particular, this approach generated a transient period of flow increase, on average peaking at ~ 20% above baseline levels within 10 min following de-occlusion, and lasting up to 0.5 h, as measured by LDF (Fig. 7A). The high variability during this hyperemic period was not conducive for accurate vasodynamic measurements, so we analyzed arterioles measured between 0.5 h and 1.5 h after reperfusion onset when RBC velocity and diameter was stabilized.

We found that arterioles dilated by ischemia were capable of constricting in response to the post-ischemic hyperemic period (31 small surface arterioles and 42 penetrating arterioles over 4 animals) (Figs. 7B to 7D); this is a result consistent with previous studies (Pinard et al. 2002). Interestingly, RBC flux after hyperemia was below baseline levels (Fig. 7E), suggesting that vasoconstriction could be involved in post-ischemic hypoperfusion in this model. Finally, dilation could be re-induced by hypercapnia (10 % CO_2 for 20 min) during a fourth period of imaging (Figs. 7B and 7D), leading to a significant increase in flux (Fig. 7E). These data confirm that penetrating arterioles were capable of active bi-directional changes in diameter following stroke.

Discussion

To examine the homeostatic function of cerebral pial arterioles following ischemia, we measured RBC flux in networks of arterioles that overly the cortical penumbra of focal stroke. Three major findings are highlighted: *i.*) While flow reversals and stalls occur in arterioles of the surface collateral network, they are not observed within penetrating arterioles. *ii.*) The change in flux of RBCs during ischemia cannot be predicted from changes in their velocity or in the lumen diameter alone. *iii.*) Small diameter surface arterioles and penetrating arterioles are the main vasoreactive components of the pial arteriole network. In our paradigm, active dilation of small arterioles compensated for incomplete recovery of RBC velocity during reperfusion to enable the full recovery of RBC flux in penetrating arterioles.

Flow pattern changes in the pial network

Previous studies characterized changes in the pattern of flow throughout arteriole networks in response to occlusion of the MCA (Schaffer et al. 2006), and with respect to peri-infarct depolarization (Pinard et al. 2002). In the present study, these flow irregularities were mapped to specific arteriole networks by using vascular casts to define arteriole connectivity beyond that observed through the imaging window (Figs. 1A and 2). Our findings indicate that flow reversals and stalls serve in the redistribution of blood to ensure homogeneous supply of penetrating arterioles during low-flow conditions. Consistent with this design, penetrating arterioles neither reversed nor stalled at any point during focal stroke. Of the total measured surface arterioles, 72% resided within loop structures or were directly connected to ACA collaterals. Despite this large fraction, blood flow reversed or stalled in only 12% of the vessels. This suggests that the occurrence of flow shifts was not limited by arteriole connectivity and that relatively few shifts were necessary to maintain homogeneous flow through penetrating arterioles during ischemia.

Determination of RBC flux in pial arterioles

The determination of RBC flux is an improvement upon *in vivo* studies that evaluate blood flow on the basis of vessel diameter alone. In particular, the measurement of only one parameter

can be misleading as the velocity of RBCs and diameter of a vessel can vary independently, particularly during disturbances of blood flow. This difficulty was explicitly noted by Kontos (Kontos 1989) and is supported by studies that show stroke-induced pial arteriole dilation alone is a poor indicator of downstream flow to tissue (Pinard et al. 2002; Tasdemiroglu et al. 1992). Our results confirm that reliance on only a single indicator of blood flow provides an incomplete description of the vascular response to stroke. In the 'Koizumu' tMCAo paradigm, RBC velocity alone suggests an incomplete recovery of blood flow during reperfusion (Figs. 3A and 3C), while diameter measurements considered alone support persistent vasodilation and therefore increased flow (Fig. 3B and 3D). The calculation of flux from these parameters (Eq. 1), however, showed that blood flow in fact recovered to baseline levels during reperfusion (Fig. 5A).

One potential caveat of our methodology is that serum flow is not measured. Indeed, serum supplies both glucose and oxygen in ischemic states, in addition to other nutritional sources. By measuring arterio-venous transit times of a fluorescent dye Rovainen *et al.* found serum flow to be on average 3-times faster than RBC flow (Rovainen et al. 1993). Serum flow may persist even when RBCs are stalled and may still represent a significant source of oxygen during ischemia (Villringer et al. 1994).

Preservation of small arteriole reactivity in the focal stroke penumbra

Our findings reveal that arteriole reactivity in the stroke penumbra remains intact and capable of modulating lumen diameter as a compensatory mechanism to conserve RBC flux at these time-points of ischemia and reperfusion. By distinguishing between the differing sizes and types of pial arterioles, the primary locus of reactivity was shown to reside in small surface arterioles and penetrating arterioles. We confirmed that small arterioles (< 23 μm) were capable of constriction in response to transient hyperemia following stroke (Figs. 7B and 7D), and thus did not become passively dilated due to loss of vascular tone. Although, we did not evaluate the arteriole response over a wide auto-regulatory curve (Kontos et al. 1978), these results nonetheless indicate that myogenic reactivity to increased flow is intact at the level of individual arterioles. Further, our findings with hypercapnic treatment (Figs. 7B and 7D) are consistent with studies that show partial preservation of reactivity to CO_2 in the stroke penumbra (Jones et al. 1989). Finally, at a histological level, parenchymal vessels within the penumbra did not bind pimonidazole during both occlusion and reperfusion periods suggesting limited hypoxic damage (Fig. 6C, left panel).

An open question is how net dilation of only smaller diameter arterioles affects pial network flow as a whole. We showed that total RBC flux into and out of these networks was conserved (Fig. 5B and 5C). However, during reperfusion the total flux available was reduced compared to baseline, consistent with incomplete recovery of flux in large surface arterioles, while penetrating arteriole flux returned to baseline (Fig. 5B). Penetrating arterioles thus extracted a larger proportion of the available blood from large supply vessels, perhaps causing a reduction in flow to watershed regions sourced by both the MCA and ACA (Momjian-Mayor and Baron 2005). This may represent a form of cerebrovascular steal, where blood flow is intercepted from the hypoperfused ischemic focus by highly collateralized and reactive penumbral regions (Scremin 1991). We suspect that unbalanced delivery of blood between the stroke penumbra and core may, in part, contribute to the poor re-oxygenation of the lateral cortex during reperfusion (Fig. 6B, right panel).

What are the long-term consequences of ischemia on penetrating arteriole reactivity? Recent work by Cipolla and colleagues suggest that isolated penetrating lenticulostriate arterioles possess normal myogenic tone and reactivity 24 h after a 1 h period of transient and moderate ischemia (Cipolla and Bullinger 2008). Interestingly, these arterioles exhibited compensatory alterations in nitric oxide and endothelial-derived hyperpolarizing factor signaling to maintain

normal vascular function. In a related study, Ngai and colleagues also found no effect on cerebral penetrating arteriole tone 24 h after 1 to 2 hrs of transient ischemia, and further demonstrated that conducted dilatory responses along penetrating arterioles were augmented following stroke (Ngai et al. 2007). These recent findings are in contrast to surface arterioles isolated from severely ischemic zones surrounding the proximal MCA, which lose tone even after 30 min of ischemia as a result of structural damage to arteriole smooth muscle (Cipolla and Curry 2002). Taken together with the results of the present study, small surface arterioles and penetrating arterioles appear to be unique in their ability to adapt and maintain regulatory function following transient ischemia. Although the mechanisms that underlie this preferential resistance to ischemia remain to be defined, the preserved reactivity of penetrating arterioles will be a key determinant for improved recovery following stroke.

Supplementary Material

Refer to Web version on PubMed Central for supplementary material.

Acknowledgments

We thank Agnieszka Prechtl for assistance with immunohistochemistry, Chris Rafie for assistance with fluorescent vascular casts, Anna Devor for surgical advice, and Jonathan Driscoll and Pablo Blinder for comments on the manuscript.

Funding: This work was funded by the Canadian Institutes of Health Research, the National Institutes of Health (NCRR, NIA, NIBIB, and NINDS), the National Science Foundation, and the Veterans Medical Research Foundation.

References

Bar T. The vascular system of the cerebral cortex. Advances in Anatomy, Embryology, and Cellular Biology 1980;59:1–62.

Barfod C, Akgoren N, Fabricius M, Dirnagl U, Lauritzen M. Laser-Doppler measurements of concentration and velocity of moving blood cells in rat cerebral circulation. Acta Physiol Scand 1997;160:123–132. [PubMed: 9208038]

Cipolla MJ, Bullinger LV. Reactivity of Brain Parenchymal Arterioles after Ischemia and Reperfusion. Microcirculation 2008;15:495–501. [PubMed: 19086259]

Cipolla MJ, Curry AB. Middle cerebral artery function after stroke: The threshold duration of reperfusion for myogenic activity. Stroke 2002;33:2094–2099. [PubMed: 12154269]

Cipolla MJ, Lessov N, Hammer ES, Curry AB. Threshold duration of ischemia for myogenic tone in middle cerebral arteries: Effect on vascular smooth muscle actin. Stroke 2001;32:1658–1664. [PubMed: 11441216]

Cipolla MJ, Li R, Vitullo L. Perivascular innervation of penetrating brain parenchymal arterioles. Journal of Cardiovasculature Pharmacology 2004;44:1–8.

Devor A, Tian P, Nishimura N, Teng IC, Hillman EM, Narayanan SN, Ulbert I, Boas DA, Kleinfeld D, Dale AM. Suppressed neuronal activity and concurrent arteriolar vasoconstriction may (the) explain negative blood oxygenation level-dependent signal. Journal of Neuroscience 2007;27:4452–4459. [PubMed: 17442830]

Dirnagl U, Pulsinelli W. Autoregulation of cerebral blood flow in experimental focal brain ischemia. J Cereb Blood Flow Metab 1990;10:327–336. [PubMed: 2329121]

Dirnagl U, Villringer A, Einhaupl KM. *In-vivo* confocal scanning laser microscopy of the cerebral microcirculation. Journal of Microscopy 1992;165:147–157. [PubMed: 1552568]

Eger EI 2nd. Isoflurane: a review. Anesthesiology 1981;55:559–576. [PubMed: 7027831]

Heistad, DD.; Kontos, HA., editors. Cerebral circulation. Bethesda: American Physiological Society; 1983.

Iadecola, C. Cerebral circulatory dysregulation in ischemia. In: Ginsberg, MD., editor. Cerebrovascular disease: pathophysiology, diagnosis, and management. Malden: Blackwell Publishing; 1998. p. 319-332.

Jones SC, Bose B, Furlan AJ, Friel HT, Easley KA, Meredith MP, Little JR. CO2 reactivity and heterogeneity of cerebral blood flow in ischemic, border zone, and normal cortex. Am J Physiol 1989;257:H473–482. [PubMed: 2504058]

Kleinfeld, D.; Friedman, B.; Lyden, PD.; Shih, AY. Targeted occlusion to surface and deep vessels in neocortex via linear and nonlinear optical absorption. In: Chen, J.; Xu, Z.; Xu, XM., et al., editors. Animal Models of Acute Neurological Injuries. Totowa: The Humana Press Inc; 2008. p. 169-183.

Kleinfeld D, Mitra PP, Helmchen F, Denk W. Fluctuations and stimulus-induced changes in blood flow observed in individual capillaries in layers 2 through 4 of rat neocortex. Proceedings of the National Academy of Sciences USA 1998;95:15741–15746.

Koizumi J, Yoshida Y, Nakazawa T, Ooneda G. Experimental studies of ischemic brain edema: 1. A new experimental model of cerebral embolism in rats in which recirculation can be introduced in the ischemic area. The Japanese Journal of Stroke 1986;8:1–8.

Kontos HA. Validity of cerebral arterial blood flow calculations from velocity measurements. Stroke 1989;20:1–3. [PubMed: 2911822]

Kontos HA, Wei EP, Navari RM, Levasseur JE, Rosenblum WI, Patterson JLJ. Responses of cerebral arteries and arterioles to acute hypotension and hypertension. American Journal of Physiology 1978;234:H371–383. [PubMed: 645875]

Lipton P. Ischemic cell death in brain neurons. Physiological Review 1999;79:1431–1568.

Longa EZ, Weinstein PR, Carlson S, Cummins R. Reversible middle cerebral artery occlusion without craniectomy in rats. Stroke 1989;20:84–91. [PubMed: 2643202]

Marshall RS. The functional relevance of cerebral hemodynamics: why blood flow matters to the injured and recovering brain. Curr Opin Neurol 2004;17:705–709. [PubMed: 15542979]

Momjian-Mayor I, Baron JC. The pathophysiology of watershed infarction in internal carotid artery disease: review of cerebral perfusion studies. Stroke 2005;36:567–577. [PubMed: 15692123]

Ngai AC, Nguyen TS, Meno JR, Britz GW. Postischemic augmentation of conducted dilation in cerebral arterioles. Stroke 2007;38:124–130. [PubMed: 17122418]

Ngai AC, Winn HR. Estimation of shear and flow rates in pial arterioles during somatosensory stimulation. Am J Physiol 1996;270:H1712–1717. [PubMed: 8928878]

Nguyen QT, Tsai PS, Kleinfeld D. MPScope: A versatile software suite for multiphoton microscopy. Journal of Neuroscience Methods 2006;156:351–359. [PubMed: 16621010]

Nishimura B, Schaffer CB, Friedman B, Lyden PD, Kleinfeld D. Penetrating arterioles are a bottleneck in the perfusion of neocortex. Proceedings of the National Academy of Sciences USA 2007;104:365–370.

Nishimura N, Schaffer CB, Friedman B, Tsai PS, Lyden PD, Kleinfeld D. Targeted insult to individual subsurface cortical blood vessels using ultrashort laser pulses: Three models of stroke. Nature Methods 2006;3:99–108. [PubMed: 16432519]

Noto T, Furuichi Y, Ishiye M, Matsuoka N, Aramori I, Mutoh S, Yanagihara T, Manabe N. Temporal and topographic profiles of tissue hypoxia following transient focal cerebral ischemia in rats. Journal of Veternary Medical Science 2006;68:803–807.

Paulson OB, Strandgaard S, Edvinsson L. Cerebral autoregulation. Cerebrovasc Brain Metab Rev 1990;2:161–192. [PubMed: 2201348]

Pinard E, Nallet, MacKenzie ET, Seylaz J, Roussel S. Penumbral microcirculatory changes associated with peri-infarct depolarizations in the rat. Stroke 2002;33:606–612. [PubMed: 11823677]

Rovainen CM, Woolsey TA, Blocher NC, Wang DB, Robinson OF. Blood flow in single surface arterioles and venules on the mouse somatosensory cortex measured with videomicroscopy, fluorescent dextrans, nonoccluding fluorescent beads, and computer-assisted image analysis. Journal of Cerebral Blood Flow and Metabolism 1993;13:359–371. [PubMed: 7683023]

Schaffer CB, Friedman B, Nishimura N, Schroeder LF, Tsai PS, Ebner FF, Lyden PD, Kleinfeld D. Two-photon imaging of cortical surface microvessels reveals a robust redistribution in blood flow after vascular occlusion. Public Library of Science Biology 2006;4:258–270.

Scremin OU. Pharmacological control of the cerebral circulation. Annu Rev Pharmacol Toxicol 1991;31:229–251. [PubMed: 2064375]

Takasawa M, Moustafa RR, Baron JC. Applications of nitroimidazole in vivo hypoxia imaging in ischemic stroke. Stroke 2008;39:1629–1637. [PubMed: 18369176]

Tasdemiroglu E, Macfarlane R, Wei EP, Kontos HA, Moskowitz MA. Pial vessel caliber and cerebral blood flow become dissociated during ischemia-reperfusion in cats. American Journal of Physiology 1992;263:H533–536. [PubMed: 1510151]

Tsai, PS. Thesis (Ph D.). University of California; San Diego: 2004. All-optical histology using two photon laser scanning microscopy and ablation with ultrashort pulses.

Tsai PS, Friedman B, Ifarraguerri AI, Thompson BD, Lev-Ram V, Schaffer CB, Xiong Q, Tsien RY, Squier JA, Kleinfeld D. All-optical histology using ultrashort laser pulses. Neuron 2003;39:27–41. [PubMed: 12848930]

Tsai, PS.; Nishimura, N.; Yoder, EJ.; Dolnick, EM.; White, GA.; Kleinfeld, D. Principles, design, and construction of a two photon laser scanning microscope for *in vitro* and *in vivo* brain imaging. In: Frostig, RD., editor. In vivo Optical Imaging of Brain Function. Boca Raton: CRC Press; 2002. p. 113-171.

Villringer A, Them A, Lindauer U, Einhaupl K, Dirnagl U. Capillary perfusion of the rat brain cortex: An *in vivo* confocal microscopy study. Circulation Research 1994;75:55–62. [PubMed: 8013082]

Abbreviations

ACA	Anterior cerebral artery
CCA	Common carotid artery
ECA	External carotid artery
ICA	Internal carotid artery
LDF	Laser Doppler flowmetry
MCA	iddle cerebral artery
RBC	Red blood cell
SEM	Standard error of the mean
tMCAo	Transient middle cerebral artery occlusion
TPLSM	Two photon laser scanning microscopy

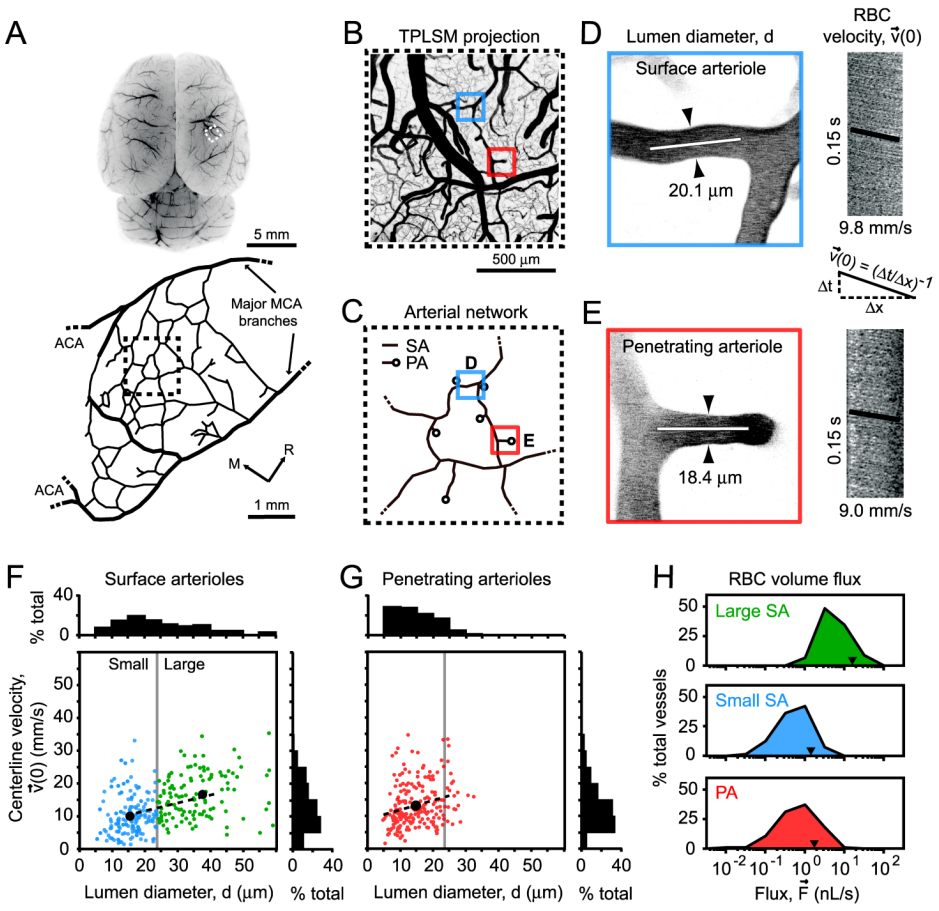

Figure 1. Vascular parameters of individual pial arterioles under basal conditions

(A) The location of the imaged region over the right dorsolateral cortex is marked (dashed square). Below, a tracing of the MCA network, derived from the vascular casting method, shows the imaged region (dashed square) relative to major distal MCA branches (thick black lines) and detailed interconnecting loop structures (thin black lines). M = medial, R = rostral. **(B)** A flattened 3-D image stack collected from the cranial window, *i.e.*, maximal Z-axis projection (300 µm depth, 5 µm steps). All TPLSM images were inverted for improved contrast of the vasculature. **(C)** Arteriole tracing of the imaged region, which reveals surface arterioles (SA) and penetrating arterioles (PA) that were randomly sampled. The analysis of a typical surface arteriole (blue square) and penetrating arteriole (red square) is shown. **(D and E)** Lumen diameter, d, was measured from maximal projections of planar 3-D image stacks (distance between arrowheads). Line-scans were repeatedly collected from the arteriole centerline axis (white line) and stacked sequentially to form a space-time image. The streaks within the line-scan image represent non-fluorescent RBC moving through a fluorescent background, with the x-axis representing the distance traveled by the RBCs, x, and the y-axis representing time, t. Centerline RBC velocity, $\vec{v}(0)$, was then calculated from the inverse of the slope of the RBC streaks, as shown in the equation. **(F and G)** Centerline velocity of RBCs from three categories of arterioles: large surface arterioles, small surface arterioles and penetrating arterioles, plotted as a function of lumen diameter. The mean velocity and diameter of each arteriole category (black circle) and linear fit (dotted line) are shown. **(H)** Histogram of the range of RBC fluxes, and average flux (arrowhead), for each arteriole category.

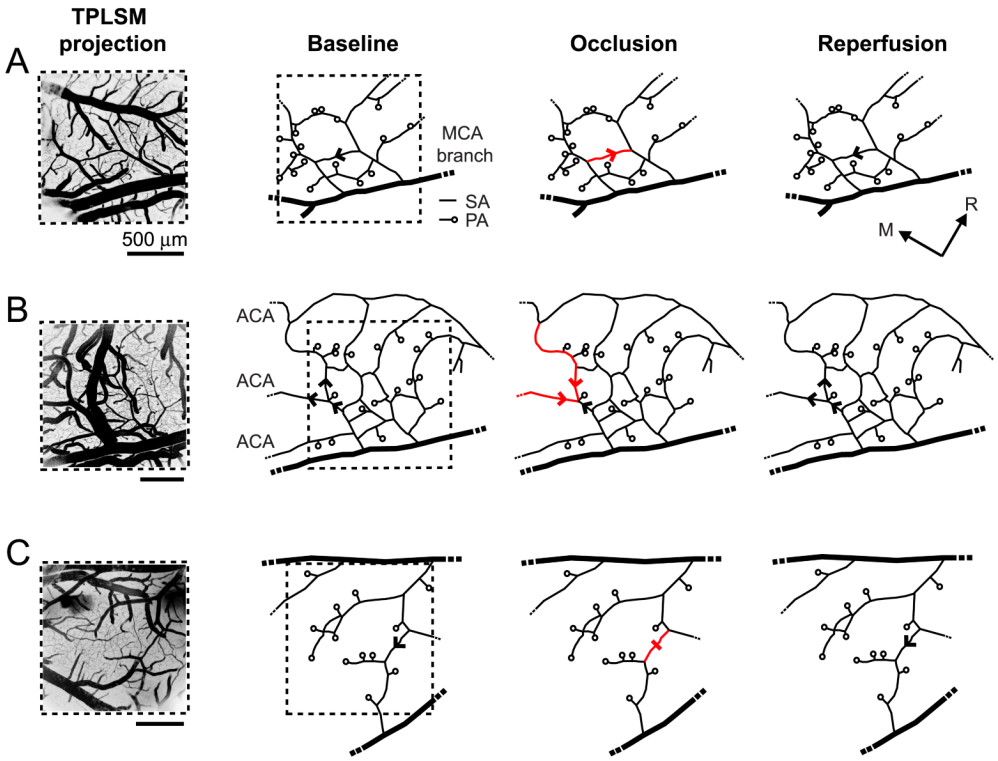

Figure 2. Shifting of RBC flow patterns in surface arteriole networks during tMCAo

Arrowheads indicate direction of blood flow in arteriole networks. Flow reversals (red arrowhead) and a stall (red dash) caused by MCA occlusion are highlighted. **(A)** Representative example of flow reversal within a small arteriole loop. **(B)** Flow reversal in large arterioles that formed anastomoses between ACA and MCA territories. **(C)** Stalling of flow in arteriole that connected perfusion between two major MCA branches.

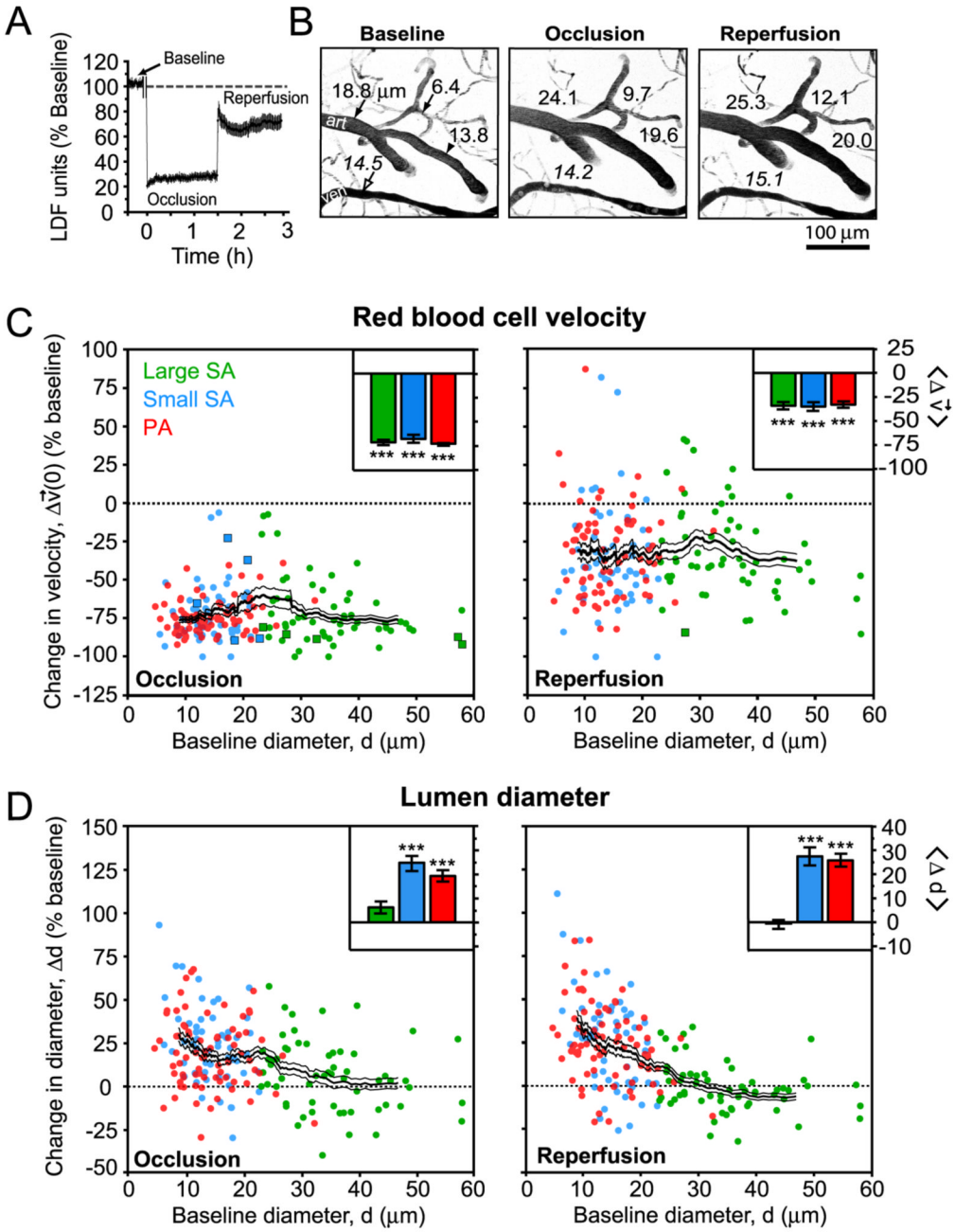

Figure 3. Change in RBC velocity and lumen diameter during tMCAo

(A) Relative changes in LDF signal from the cranial window in the 'Koizumi' model of tMCAo (Koizumi et al. 1986). LDF data represents mean ± SEM from n = 8 animals. An approximately 10 min period during the filament insertion was omitted from the trace. **(B)** Robust stroke-induced vasodilation in a network of small surface arterioles and penetrating arterioles. The images are maximal projections of 100 µm deep image stacks with 5 µm steps. Lumen diameters, in µm, of surface arterioles (filled arrows), a penetrating arteriole (filled arrowhead), and a venule (open arrow) are shown at each stage of tMCAo. **(C)** Change in RBC velocity during occlusion and reperfusion plotted as a function of baseline diameter. Square data points represent arterioles with reversed or stalled flow with respect to baseline. **(D)** Change in lumen

diameter during occlusion and reperfusion plotted as a function of baseline diameter. For C and D, a running average ± SEM (40 vessel window) is overlaid. Inset bar graphs show mean ± SEM for each of the three vessel types. *** $p < 10^{-3}$, significantly different from baseline.

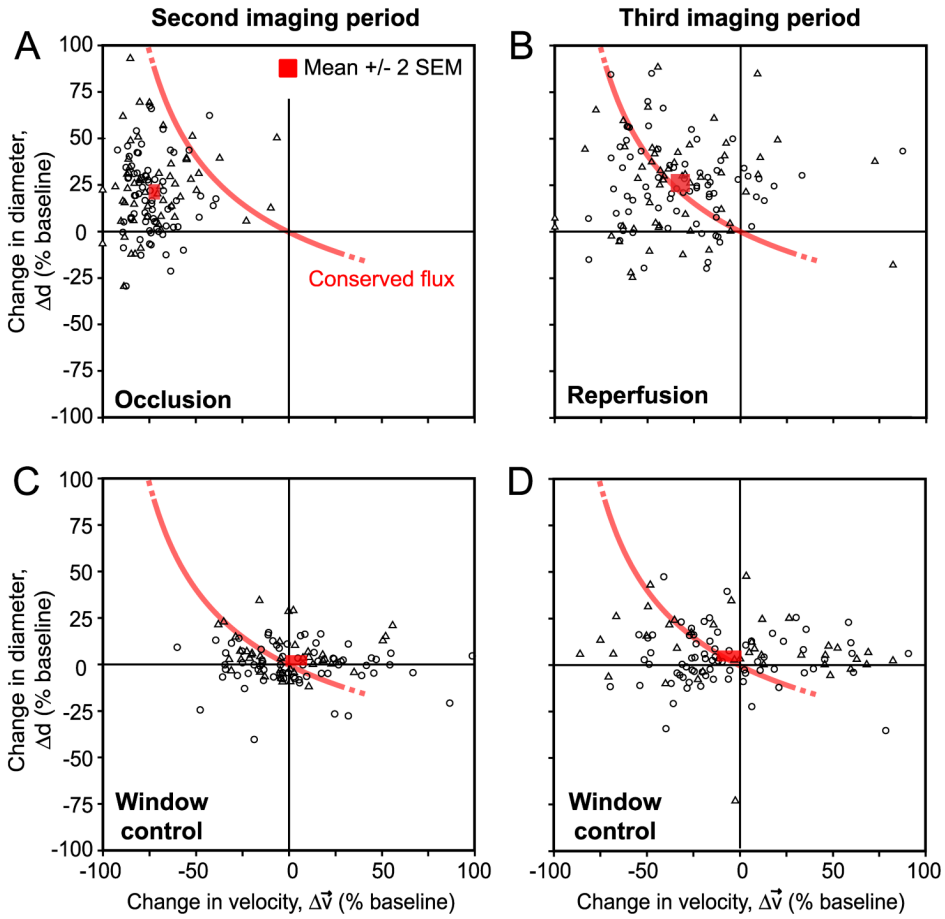

Figure 4. Vasodilation tracks RBC velocity to conserve flux during reperfusion

(A and B) Change in lumen diameter plotted as a function of change in RBC velocity during the occlusion and reperfusion periods, respectively. The interface where RBC flux is conserved, based on Eq. 2, is shown in red. All points on the curve indicate maintenance of baseline levels of flux; those to the left of the curve have substandard flux, while those to the right have enhanced flux. A red box, mean ± 2 SEM, is the mean response over all vessels. During occlusion (A), the mean response is significantly different from the closest point on the line of conserved flux; $p < 0.001$ (two-sided one sample t-test). In contrast, the mean response during reperfusion (B) is not significantly different from the line of conserved flux; $p > 0.05$ (two-sided one sample t-test). Data represents 131 small surface arterioles (triangles) and penetrating arterioles (circles) combined from 11 tMCAo experiments. Large surface arterioles were not included in this analysis. **(C and D)** Vasodynamic changes in Window control groups, *i.e.*, cranial window with no vascular manipulation, showed no significant difference from the line of conserved flux in either the second or third period of imaging; $p > 0.05$ (two-sided one sample t-test). For controls, each imaging period was maintained for the same time-span as the tMCAo experimental group, *i.e.*, 90 min. Data represents 113 small surface arterioles and penetrating arterioles combined from 6 Window control experiments.

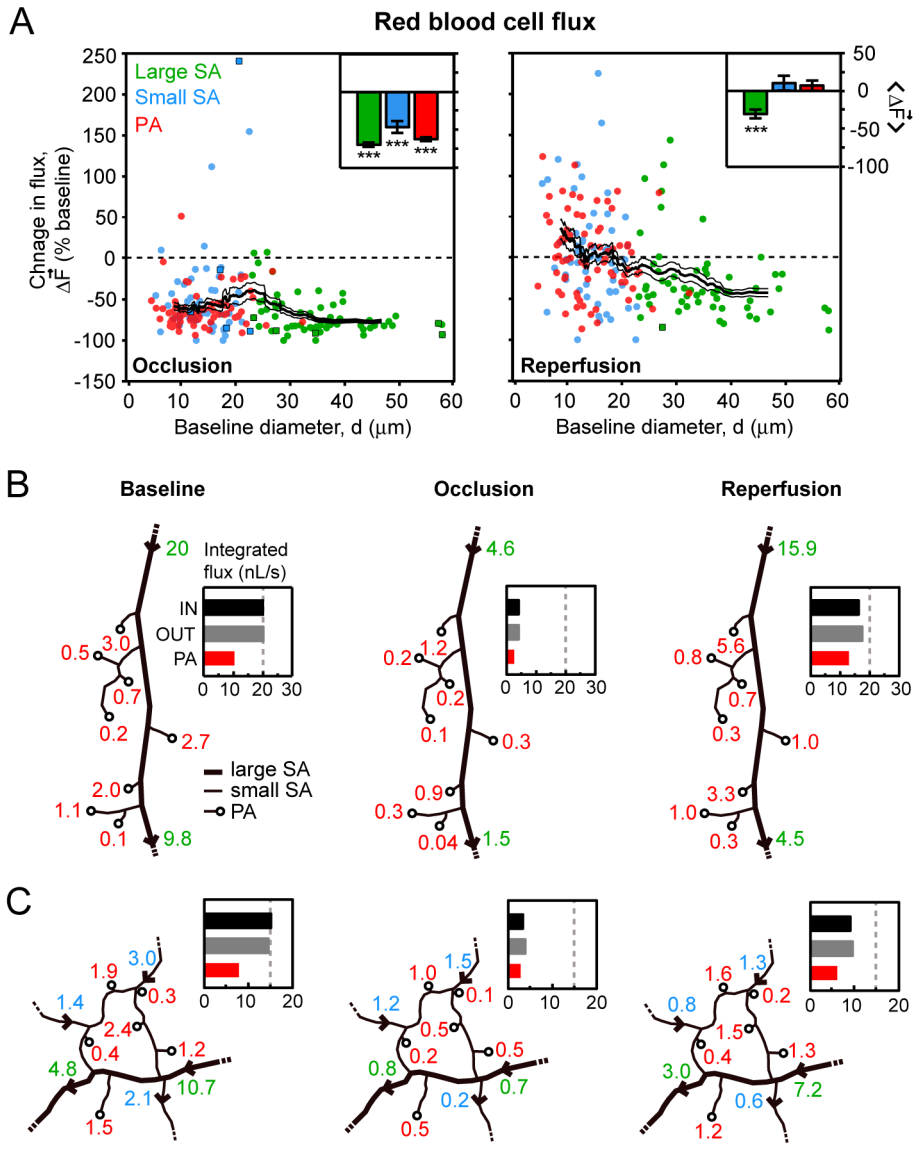

Figure 5. Change in RBC volume flux during tMCAo

(A) Change in RBC flux during occlusion and reperfusion plotted as a function of baseline diameter. Square data points represent arterioles with reversed or stalled flow with respect to baseline. A running average ± SEM (40 vessel window) is overlaid. Inset bar graphs show average change in flux ± SEM for each of the three vessel types. *** $p < 10^{-3}$, significantly different from baseline. **(B and C)** In two separate experiments, cumulative flux entering and exiting an arteriole network was measured. Arterial traces with flux values, in nL/s, are shown for each imaging period. A bar graph summarizes the net input (IN) and output (OUT) from the arteriole network during each period. Flux exiting only through penetrating arterioles (PA) is also shown.

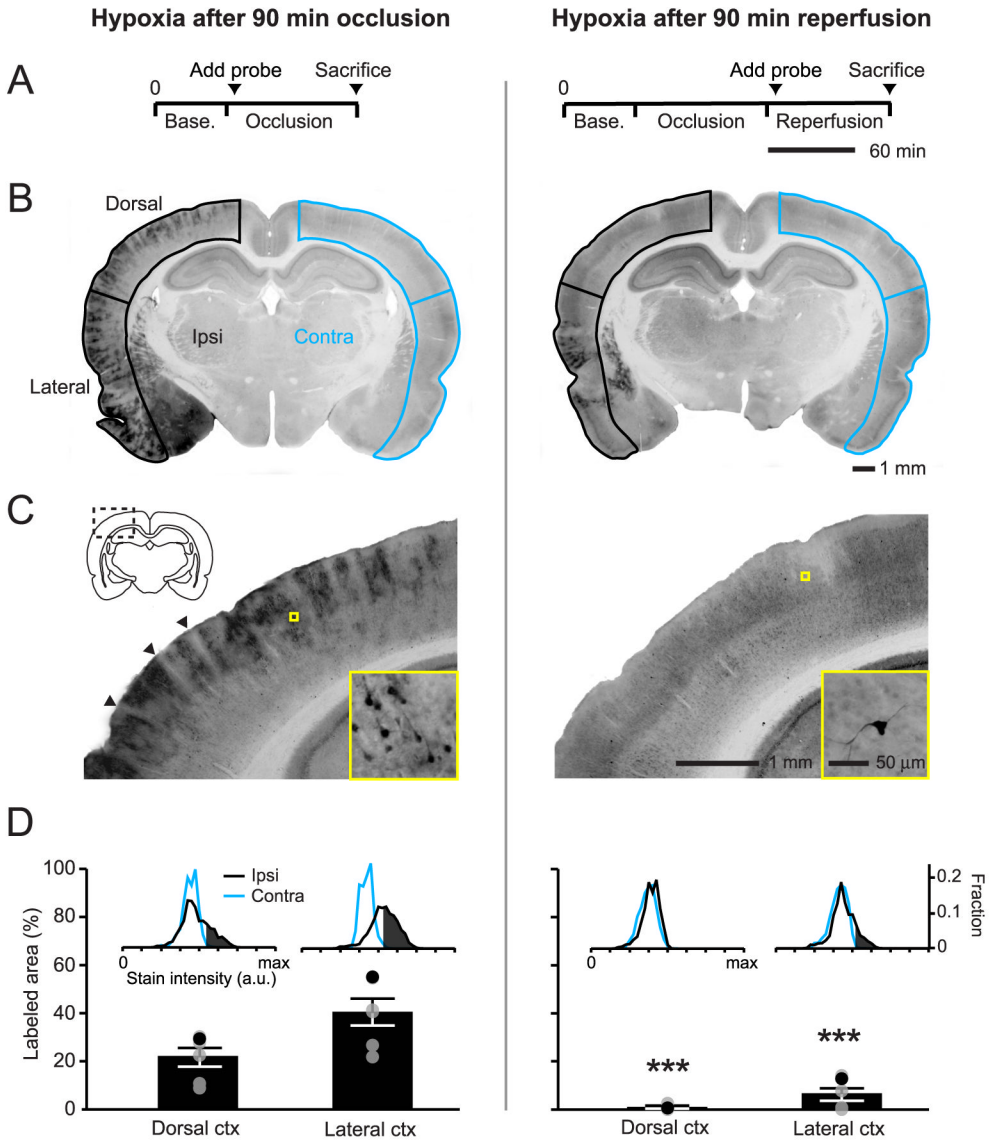

Figure 6. Absence of hypoxic tissue in the cortical penumbra during reperfusion

(A) Experimental timelines for the intra-arterial injection of pimonidazole, a marker of hypoxia. Probe circulation time between the two groups was equivalent, *i.e.*, 90 min. **(B)** Representative coronal images of pimonidazole labeling from animals injected during occlusion or reperfusion. Ipsilateral (black, ischemic side) and contralateral (blue) cortices were demarcated and separated into dorsal and lateral portions. **(C)** Magnified images of dorsal cortex (dashed rectangle), with a further magnified view of stained cells (yellow square). Arrowheads indicate relatively unstained zones surrounding penetrating vessels. **(D)** Average labeled area ± SEM expressed as percentage of total dorsal or lateral cortical area. Black points within the scatter plot represent the animal shown in the figure. Inset histograms illustrate the threshold setting used to differentiate positive staining in ipsilateral cortex from background, defined as the lower 90 % of the intensity histogram from the contralateral side (see also Materials and Methods). *** $p < 0.001$, significantly different from the group injected at occlusion (unpaired t-test).

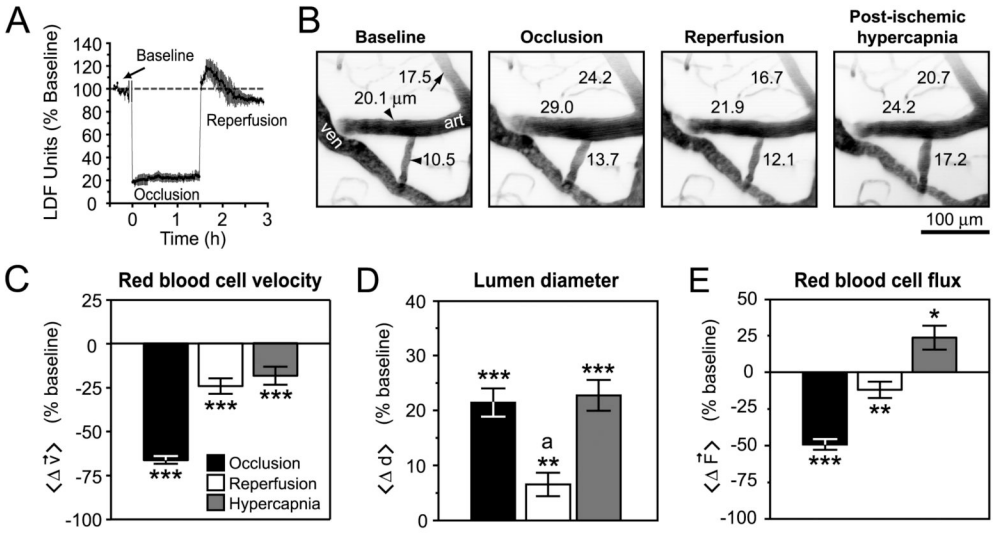

Figure 7. Active vascular responses to post-ischemic hyperemia and hypercapnia

(A) LDF measurements reveal a period of hyperemia after reperfusion in the 'Longa' model of tMCAo (Longa et al. 1989). LDF data represents mean ± SEM from n = 3 animals. An approximately 10 min period during filament insertion was omitted from the trace. **(B)** Representative images of diameter changes for two penetrating arterioles (arrowheads) and a small surface arteriole (arrow) in response to occlusion, reperfusion, and hypercapnia. The images are maximal projections of 100 µm deep image stacks with 5 µm steps. (**C - E**) Average changes in measured vascular parameters for small surface arterioles and penetrating arterioles. Data represents mean ± SEM. *** $p < 10^{-3}$, ** $p < 0.01$, * $p < 0.05$ significantly different from baseline, [a] $p < 10^{-3}$, significantly different from diameter during occlusion and hypercapnia (paired t-test).